



LOW-THERMAL-MATURITY (<0.7% VR) MUDROCK PORE SYSTEMS: MISSISSIPPIAN BARNETT SHALE, SOUTHERN FORT WORTH BASIN

Robert M. Reed and Robert G. Loucks

*Bureau of Economic Geology, Jackson School of Geosciences, University of Texas at Austin,
University Station, Box X, Austin, Texas 78713–8924, U.S.A.*

ABSTRACT

Limited scanning electron microscope (SEM) analysis has been done previously on Ar-ion-milled samples of low-thermal-maturity, organic-rich mudrocks transitioning into the oil window. Using 23 samples from 12 wells, this study examines pore systems and characterizes organic matter from such mudrocks in the Mississippian Barnett Shale of the southern Fort Worth Basin. Samples, prepared using broad ion-beam (BIB) milling with Ar ions, are at relatively low thermal maturities of 0.4 to 0.6% vitrinite reflectance (VR). Lithologies are variable, but are generally more argillaceous and less siliceous than those in the northeastern Fort Worth Basin.

Pores in mudrocks can be classified into three types: organic-matter, interparticle, and intraparticle. Variable development of all three types has been observed in studied samples. Organic matter occurs primarily as a fine mesh surrounding mineral grains. Few or no organic-matter pores are found in the study samples. Interparticle pores are present in some samples in areas where organic matter is absent or limited. Some interparticle pores are also found in the stress shadows around rigid grains. Intraparticle pores after dissolved grains are common in the study samples. Most of these are related to feldspars, particularly albite feldspars. Intraparticle-pore diameters range from nanometers to micrometers.

Low-thermal-maturity Barnett mudrocks have less porosity than originally expected because of the extreme ductility of kerogen, which has flowed into interparticle-pore spaces during compaction. Most of the pore volume is represented by intraparticle pores (dissolved grains), but there are some interparticle pores present, particularly between clay mineral grains. Organic-matter pores are very rare to absent at vitrinite reflectance less than 0.75% in the Barnett Shale.

INTRODUCTION

Pore networks of ion-milled samples of very low-thermal-maturity mudrocks (virtually sediments) have been studied (Milliken and Reed, 2010; Day-Stirrat et al., 2012, 2013; Emmanuel and Day-Stirrat, 2012; Milliken et al., 2014) using the scanning electron microscope (SEM). Pore networks of higher-thermal-maturity mudrocks have also been extensively documented using ion-milled samples (e.g., Loucks et al., 2009; Ambrose et al., 2010; Curtis et al., 2010; Chalmers et al., 2012; Milliken et al., 2012, 2013; Cardott et al., 2015; Klaver et al., 2015). However, less SEM analysis of these milled samples has been done on low-thermal-maturity, organic-rich mudrocks transitioning into the oil window (e.g., Fishman et al., 2012; Klaver et al., 2012). The objective of this study is to examine pore networks

and characterize organic-matter behavior from a suite of organic-bearing mudrocks from the Mississippian Barnett Shale of the southern Fort Worth Basin (Fig. 1).

BACKGROUND

This study collected data from 12 shallow cores that completely penetrated the Barnett Shale section (Figs. 1 and 2). Twenty-three ion-milled samples collected from these cores were examined using the SEM. Current depth of burial of these mudrocks ranges from 190 ft to 2409 ft; depth of burial generally increases to the northeast across the study area (Fig. 1). Thickness of the Barnett Shale in these cores ranges up to 200 ft and shows a slight trend of northeast thickening. The thickness in the study area contrasts with the productive area of the northeastern Fort Worth Basin, where the average thickness of the unit is 550 ft (Loucks and Ruppel, 2007). In the southern part of the Fort Worth Basin, the Barnett Shale overlies Mississippian rocks of either the Whites Crossing or Chappel limestones and is overlain by the Pennsylvanian Marble Falls Limestone (Fig. 3).

In terms of thermal maturity of the study area, past interpretations have been partly speculative. Pollastro et al. (2007)

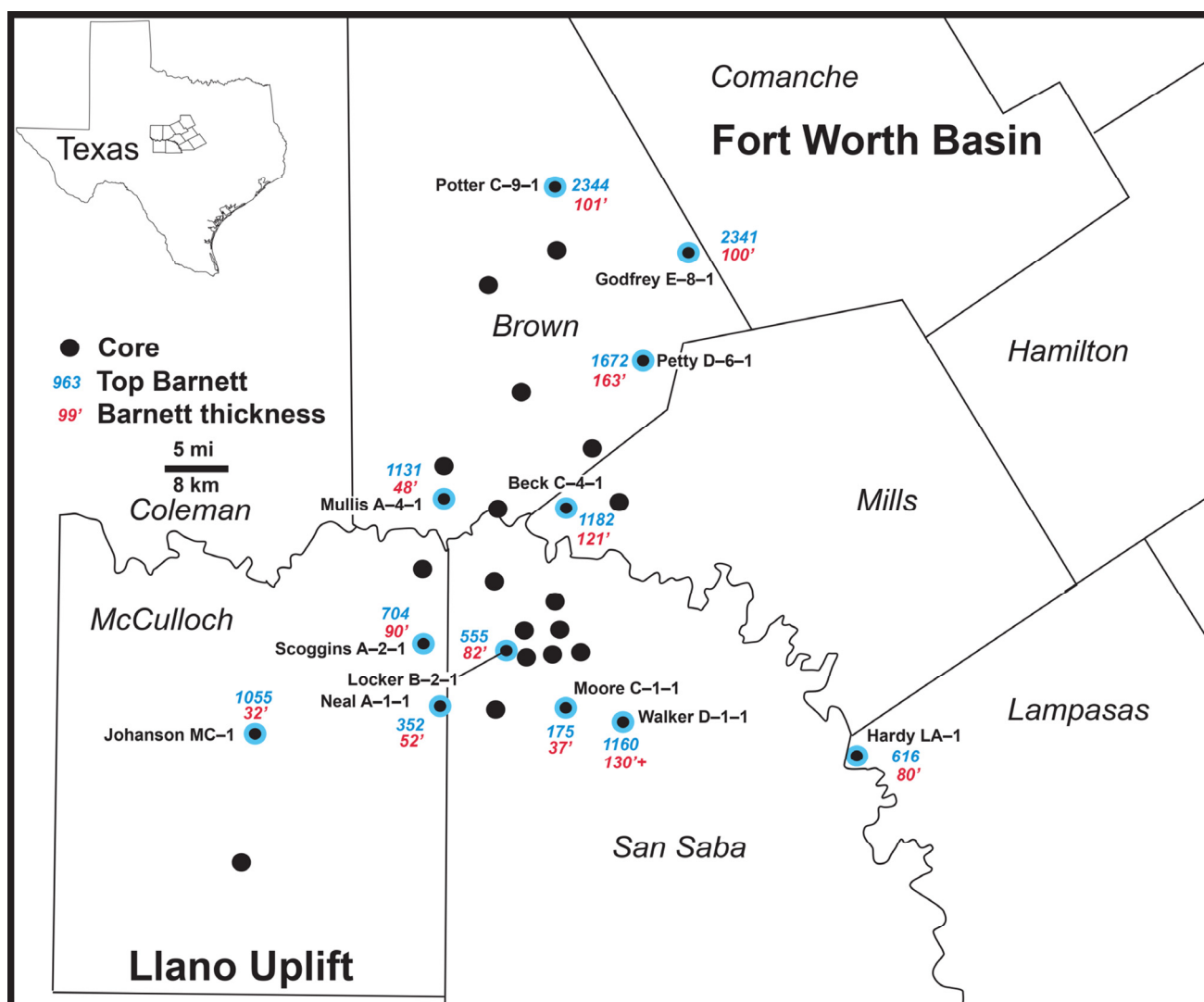


Figure 1. Map showing the location of sampled wells (blue outlined black dots) from the southern part of the Fort Worth Basin. Inset map shows location within Texas.

placed the Barnett section of the study area below 0.7% vitrinite reflectance (VR) and estimate that some parts of the area could be below 0.5% VR (Fig. 2) based on limited thermal data. Romero-Sarmiento et al. (2013) used thermal modeling to predict slightly higher, but still low, thermal maturities for the study area. Bernard et al. (2012) determined that one sample from an outcrop in the southern Fort Worth Basin had a Rock-Eval Tmax of 420°C, which gives a calculated thermal maturity of 0.4% VRc. They also determined that this sample had organic matter that was entirely kerogen (no conversion to bitumen).

METHODS

SEM samples were prepared for examination using broad ion-beam (BIB) milling with Ar ions. Two different milling machines were used. Early in the study, samples were prepared using a Gatan Model 682 Precision Etching and Coating System (PECS) equipped with a slope cutter attachment. These samples were milled primarily using an accelerating voltage of 5 kV, a sample current of 350 mA, and a milling time of 24 hr. Because of the mechanics of the equipment, these samples were generally milled at a 30- or 45-degree angle to bedding. Later in the study, samples were prepared using a Leica EM Triple Ion-Beam Cutter (TIC) 020 system. These samples were milled using an accelerating voltage of 8 kV, a source current of 2.8 mA, and a milling

time of 10 hr. In most cases, these samples were milled perpendicular to bedding. All BIB-milled samples were given a 4- to 6-nm coating of Ir to prevent charge buildup during SEM examination.

Different BIB-milled samples were imaged using one of two field-emission SEM's. Early samples were imaged on a Zeiss Supra 40VP SEM, and later samples were imaged on an FEI Nova NanoSEM 430 SEM equipped with dual Bruker XFlash[®] SDD energy dispersive spectroscopy (EDS) systems for element identification and mapping. Moderate accelerating voltages (5–15 kV) were used on these systems to avoid causing beam damage to the samples. SEM working distances for imaging were 4 to 6.5 mm.

Material from the same depth as some BIB-milled samples was analyzed for LECO total organic carbon (TOC) and Rock-Eval pyrolysis by Humble Geochemistry or by GeoMark Research. Some additional samples from these wells that were not BIB milled were also analyzed for LECO TOC and Rock-Eval pyrolysis and have been included in the thermal-maturity dataset (Table 1).

THERMAL MATURITY AND COMPOSITION

The cores in this study are at relatively low thermal maturities of 0.4 to 0.6% VRc, calculated from Rock-Eval Tmax (Fig.

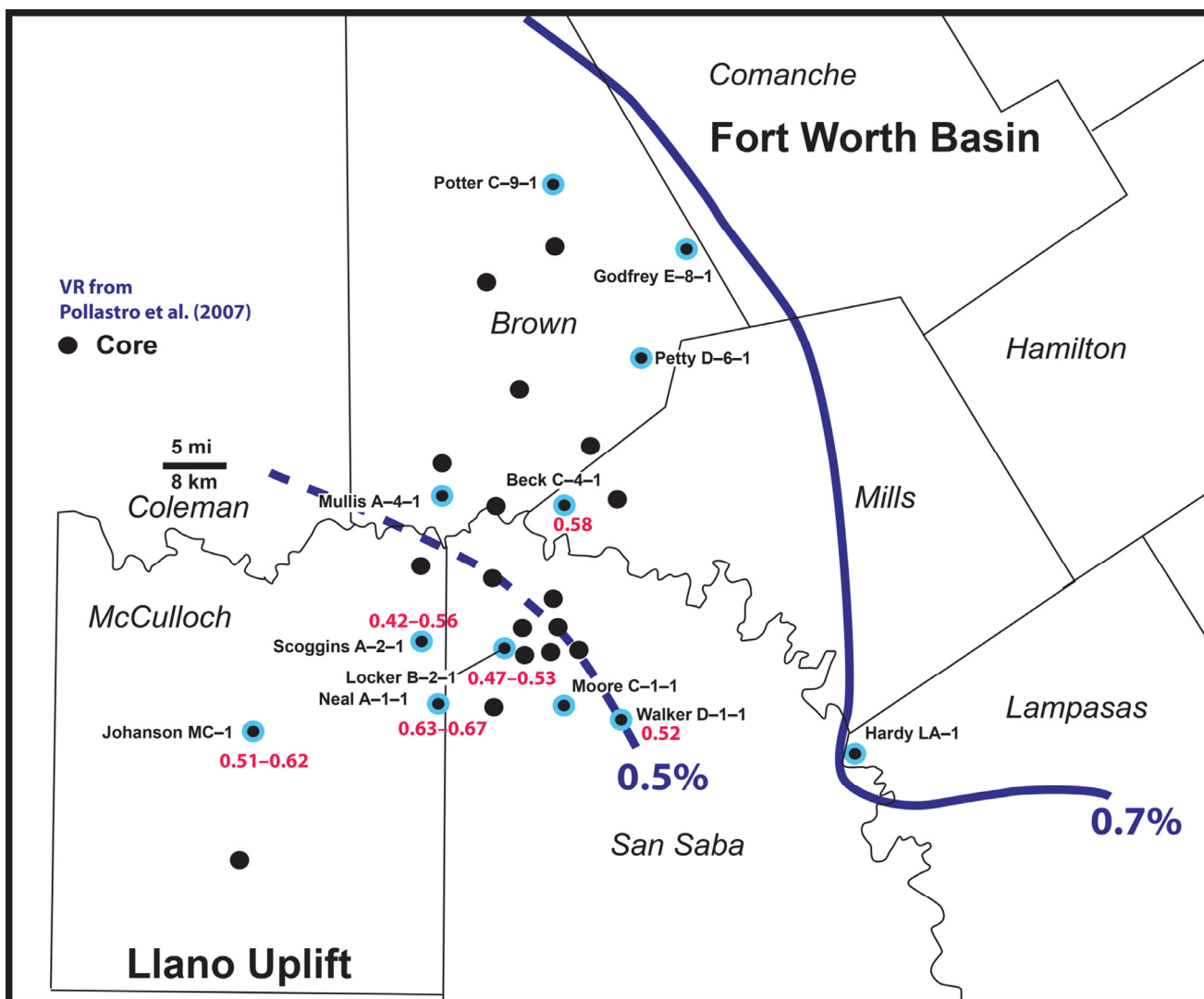


Figure 2. Map showing calculated vitrinite reflectance (VRc) ranges (red numbers) from some sampled wells as well as from previous thermal maturity estimates. Value for the Walker D-1-1 well is an unpublished vitrinite reflectance (VRo) value measured by the U.S. Geological Society.

2; Table 1) using the equation of Jarvie et al. (2001). Although previous workers (Pollastro et al., 2007) predicted an overall increase in thermal maturity to the northeast, our new data suggest a more complex scenario showing a lower-thermal-maturity area in the south flanked by higher values (Fig. 2). However, given uncertainties inherent in VRc due to complications in the measurement of Tmax (Peters, 1986), little or no thermal gradient may be present across the study area. In particular, Tmax values from the Neal well (Table 1; Fig. 2) may be anomalously high because of the probable Type III kerogen dominant in these samples (Peters, 1986). S1 values from Rock-Eval pyrolysis (Table 1) show that most of the samples contain limited amounts of extractable hydrocarbons, suggesting a thermal history transitional into the oil window.

Total organic carbon (TOC) of sampled rocks from these cores ranges from 0.9 to 12.7% (Table 1). This is similar to the TOC range seen in the more deeply buried, productive areas of the Fort Worth Basin (Loucks and Ruppel, 2007).

Sample lithologies are variable, but are generally more argillaceous and less siliceous than those common in the northern part of the Fort Worth Basin (Loucks and Ruppel, 2007) (Fig. 4). Most samples show a mix of silt-sized grains consisting of feldspars, quartz, and carbonates with a clay mineral matrix (Fig. 5).

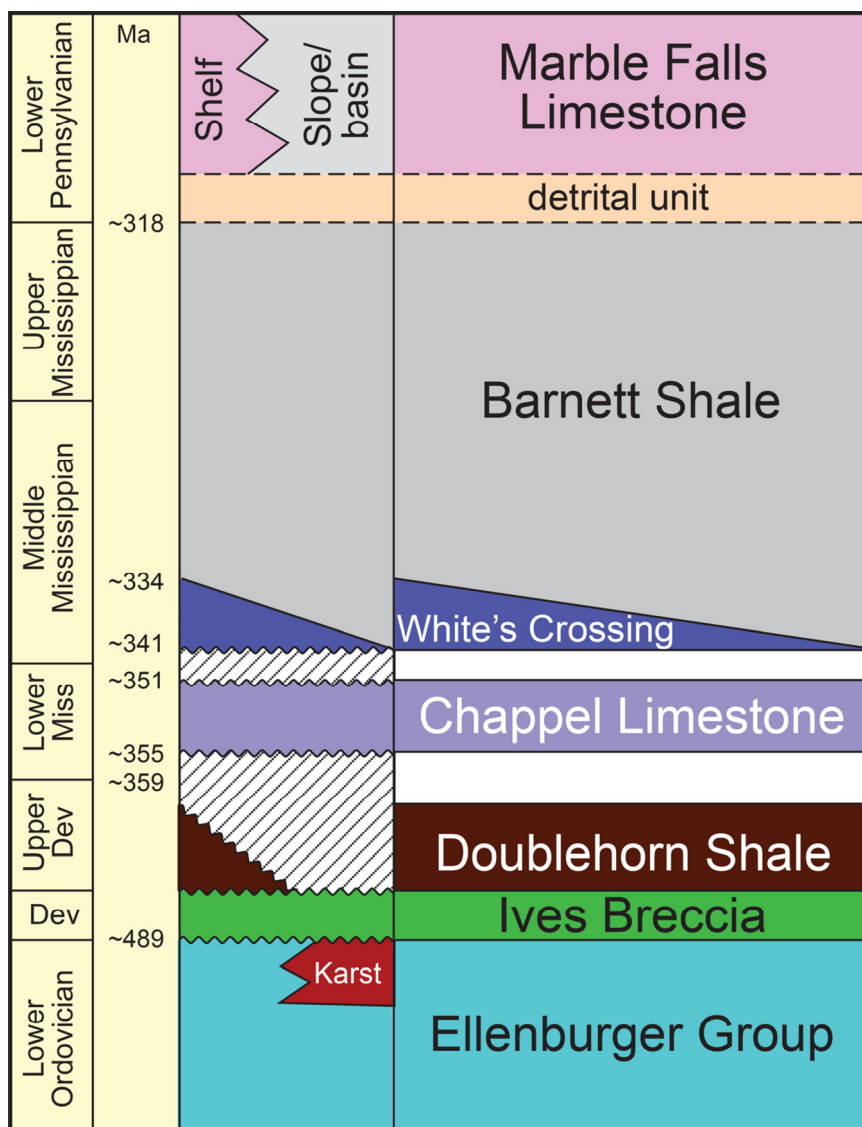
Some samples contain more carbonate (Fig. 5A) and some less (Fig. 5B). Calcite is present in varying amounts in most samples; dolomite is present only in some (Fig. 5C). Some samples contain significant amounts of phosphate (Fig. 5D), although the most phosphate-rich layers were avoided during sampling, as they are generally minor.

PORE AND ORGANIC-MATTER OBSERVATIONS

Pores in mudrocks can be divided into three groups: organic-matter, interparticle, and intraparticle (Loucks et al., 2012). According to Loucks et al. (2012), organic-matter pores are pores within organic matter, whether in-place or migrated, interparticle pores are pores between particles, and intraparticle pores are pores within a particle or within a composite particle boundary. Variable development of all three types has been observed in samples from this study.

Few or no organic-matter pores are found in the low-thermal-maturity samples in this study, which is consistent with previous observations of the Barnett Shale (Loucks et al., 2009). The few organic-matter pores that are found are typically associated with either pyrite (Fig. 6A) or, more rarely, sphalerite.

Figure 3. Stratigraphic column of the southern Fort Worth Basin.



Where present, organic-matter pores are typically in the nanometer to tens-of-nanometer size range and have bubble-like morphologies (Fig. 6A).

Although organic-matter pores are few, the behavior and abundance of the organic matter in these samples have a profound influence on the development of pore networks in the samples. Organic matter occurs both as a fine mesh surrounding mineral grains (Figs. 5 and 6) and as grainlike morphologies (equant shape, diameters larger than a micrometer; Fig. 6B). The fine mesh seems to have formed through compaction of the original ductile kerogen in the rocks. Textural evidence (Loucks and Reed, 2014) in our samples supports kerogen as the dominant organic matter, except in a few higher-maturity samples (~0.7% VR) that contain some migrated bitumen (Fig. 7). Flow caused by ductile deformation during compaction of kerogen into interparticle pores has greatly reduced the porosity present in these samples.

Interparticle pores are present in some samples in layers where organic matter is absent or limited (Fig. 8). Some interparticle pores are also preserved in the stress shadows around rigid grains of both silt and clay size (Schneider et al., 2011). Interparticle pores range in size from nanometers to micrometers, although most are less than a micrometer in diameter. Many interparticle pores have distinctive triangular outlines. A tendency for mudrocks that are organic poor to also be clay-rich limits

interparticle pore size and number. In clay-rich areas that are also free of organic matter, interparticle and intraparticle pores within clays can be difficult to distinguish (Fig. 8A).

Intraparticle pores representing dissolved and/or replaced silt-sized grains are common in the mudrock samples from this study. Most of these are related to either dissolved feldspar grains (Fig. 9) or what may have been chemically unstable rock fragments (Fig. 10). In some cases, detrital feldspar grains have been completely or partially replaced by diagenetic albite and/or calcite (Figs. 9A–9D). In other cases, complete dissolution appears to have occurred with subsequent growth of diagenetic minerals into the open space (Figs. 10A and 10B). In still other cases, grains that were probably rock fragments have been replaced by diagenetic clays (Fig. 10C) that incompletely refill the former grain mold. A wide range of minor or complete dissolution/precipitation is present, but most grains show significant dissolution. Sizes of intraparticle pores in dissolved or replaced grains vary widely from nanometers to micrometers. The pore-containing grains are generally at least partially surrounded by a mesh of organic matter (Fig. 6C), suggesting that compaction and/or flow of organic matter was largely complete before grain dissolution.

Intraparticle pores related to the dissolution of carbonate commonly have been observed in other mudrock formations (Schieber, 2010; Loucks et al., 2012; Fishman et al., 2012).

Table 1. Rock-Eval pyrolysis and calculated vitrinite reflectance data.

| Well Name | County | Depth (ft) | Formation Name | LECO TOC | S1 | S2 | S3 | Tmax (°C) | Calc. %VR | HI | OI | S2/S3 | S1/TOC | PI |
|----------------------|-----------|------------|----------------|----------|------|-------|------|-----------|-----------|-----|----|-------|--------|------|
| Neal A-1-1 | McCulloch | 362 | Barnett | 0.95 | 0.05 | 0.31 | 0.30 | 433 | 0.63 | 33 | 32 | 1 | 5 | 0.14 |
| Neal A-1-1 | McCulloch | 396 | Barnett | 2.36 | 0.08 | 1.15 | 0.81 | 435 | 0.67 | 49 | 26 | 2 | 3 | 0.07 |
| Locker B-2-1 | San Saba | 603.1 | Barnett | 3.75 | 0.75 | 22.67 | 0.78 | 424 | 0.47 | 605 | 21 | 29 | 20 | 0.03 |
| Locker B-2-1 | San Saba | 628.25 | Barnett | 7.07 | 1.65 | 49.03 | 1.11 | 427 | 0.53 | 693 | 16 | 44 | 23 | 0.03 |
| C.D. Scoggins A-2-1 | McCulloch | 767 | Barnett | 7.57 | 2.70 | 54.54 | 0.82 | 424 | 0.47 | 720 | 11 | 67 | 36 | 0.05 |
| C.D. Scoggins A-2-1 | McCulloch | 789 | Barnett | 3.89 | 0.59 | 18.12 | 0.37 | 421 | 0.42 | 466 | 10 | 49 | 15 | 0.03 |
| C.D. Scoggins A-2-1 | McCulloch | 793 | Barnett | 4.21 | 0.91 | 25.28 | 0.57 | 429 | 0.56 | 600 | 14 | 44 | 22 | 0.03 |
| Harold Johanson MC-1 | McCulloch | 1068 | Barnett | 3.05 | 0.68 | 14.79 | 0.49 | 430 | 0.58 | 485 | 16 | 30 | 22 | 0.04 |
| Harold Johanson MC-1 | McCulloch | 1070 | Barnett | 3.17 | 0.56 | 17.62 | 0.48 | 432 | 0.62 | 556 | 15 | 37 | 18 | 0.03 |
| Harold Johanson MC-1 | McCulloch | 1073 | Barnett | 2.72 | 0.35 | 10.44 | 0.42 | 431 | 0.60 | 384 | 15 | 25 | 13 | 0.03 |
| Harold Johanson MC-1 | McCulloch | 1086 | Barnett | 12.72 | 2.59 | 70.93 | 1.39 | 426 | 0.51 | 558 | 11 | 51 | 20 | 0.04 |
| Beck C-4-1 | Mills | 1254.33 | Barnett | 3.75 | 0.95 | 23.60 | 0.59 | 430 | 0.58 | 629 | 16 | 40 | 25 | 0.04 |
| Beck C-4-1 | Mills | 1270 | Barnett | 3.08 | 1.02 | 19.92 | 0.58 | 430 | 0.58 | 647 | 19 | 34 | 33 | 0.05 |

TOC = weight percent organic carbon; S1, S2 = mg of hydrocarbons per gram of rock; S3 = mg of CO₂ per gram of rock; HI = hydrogen index = mg hydrocarbons per gram of TOC; OI = oxygen index = mg of CO₂ per gram of TOC; and PI = production index = S1 / (S1 + S2). VR calculated from Tmax using the equation of Jarvie et al. (2001).

However, in the Barnett mudrocks from the present study, few carbonate grains showing dissolution-related intraparticle pores were noted. Where present, carbonate intraparticle pores seem unrelated to dissolution, but rather are either fluid inclusions or relict interparticle pores that have been included in recycled grains (Fig. 11). Intraparticle pores related to dissolution of TiO₂ grains (probably rutile) have been observed but are not volumetrically important.

Sampling avoided minor concentrated phosphatic layers. However, some phosphatic material was observed in several samples as isolated grains (Fig. 12A) or discontinuous elongate lenses (compacted pellets?; Figs. 5D and 12B). Typically this phosphatic material has intraparticle pores in the hundreds-of-nanometers size range. In areas that were probably pellets, the intraparticle pores have connectivity and morphology more typical of interparticle pores (Fig. 12B).

Intraparticle pores related to pyrite framboids have been noted previously in the Barnett Shale (e.g., Loucks et al., 2009, 2012). However, most of the intercrystalline spaces in framboids from these low-maturity rocks are filled with organic matter (Fig. 6A). A few small (nanometer-scale) pores are present in some pyrite framboids that do not contain organic matter.

In most samples, the primary observation about pores is their limited presence. The majority of pores present are the isolated intraparticle pores related to dissolution of unstable grains such as feldspar. Nearly all of the interparticle pores have been destroyed by compaction of ductile clays and kerogen. The thermal maturity of the mudrock is too low to have generated more than a few organic-matter pores.

MICROFRACTURES

Microfractures, as defined for the purpose of this study, are fractures too small to be seen with the unaided eye (Anders et al., 2014). For Barnett mudrocks, where the natural fractures are generally filled with white calcite versus a dark matrix, this translates to small apertures (typically on the micrometer scale) for visible fractures. Much speculation, but little documentation, exists to support the existence of naturally occurring, open microfractures in most mudrock reservoirs (Gale et al., 2014).

Microfractures occur in many of the samples examined for this study. Completely open microfractures cutting through the mudrock matrix are present in various abundances (Fig. 13). The vast majority of these have dominant bedding-parallel traces. These microfractures—which typically follow grain boundaries and do not break through quartz, feldspar, or calcite silt grains—generally lack mineralization and have smooth, parallel sides (Fig. 13). The more clay-rich a sample is, the more likely it is to have these open horizontal microfractures. In several samples, gypsum-lined, bedding-parallel microfractures (Capuano, 1993; Fig. 8A) have been observed. However, these are not definitively naturally occurring; gypsum in mudrocks can form post-coring following dissolution of carbonate by acids being released through oxidation of unstable iron sulfides (Milliken and Land, 1994).

Proposed bitumen-filled, horizontal microfractures (Lash and Engelder, 2005) are difficult to distinguish from elongated or ductilely deformed pieces of kerogen (Figs. 5D and 6D). Absolute differentiation of the two possibilities hinges largely on the ability to differentiate kerogen from bitumen by means of microanalysis. The generally low thermal maturity of the samples from this study makes bitumen-filled microfractures less likely.

Based on our observations, we have not been able to definitively document any naturally occurring microfractures in these low-thermal-maturity Barnett mudrocks. Open microfractures that do occur are interpreted as artifacts relating either to post-coring pressure release or desiccation during long-term core storage.

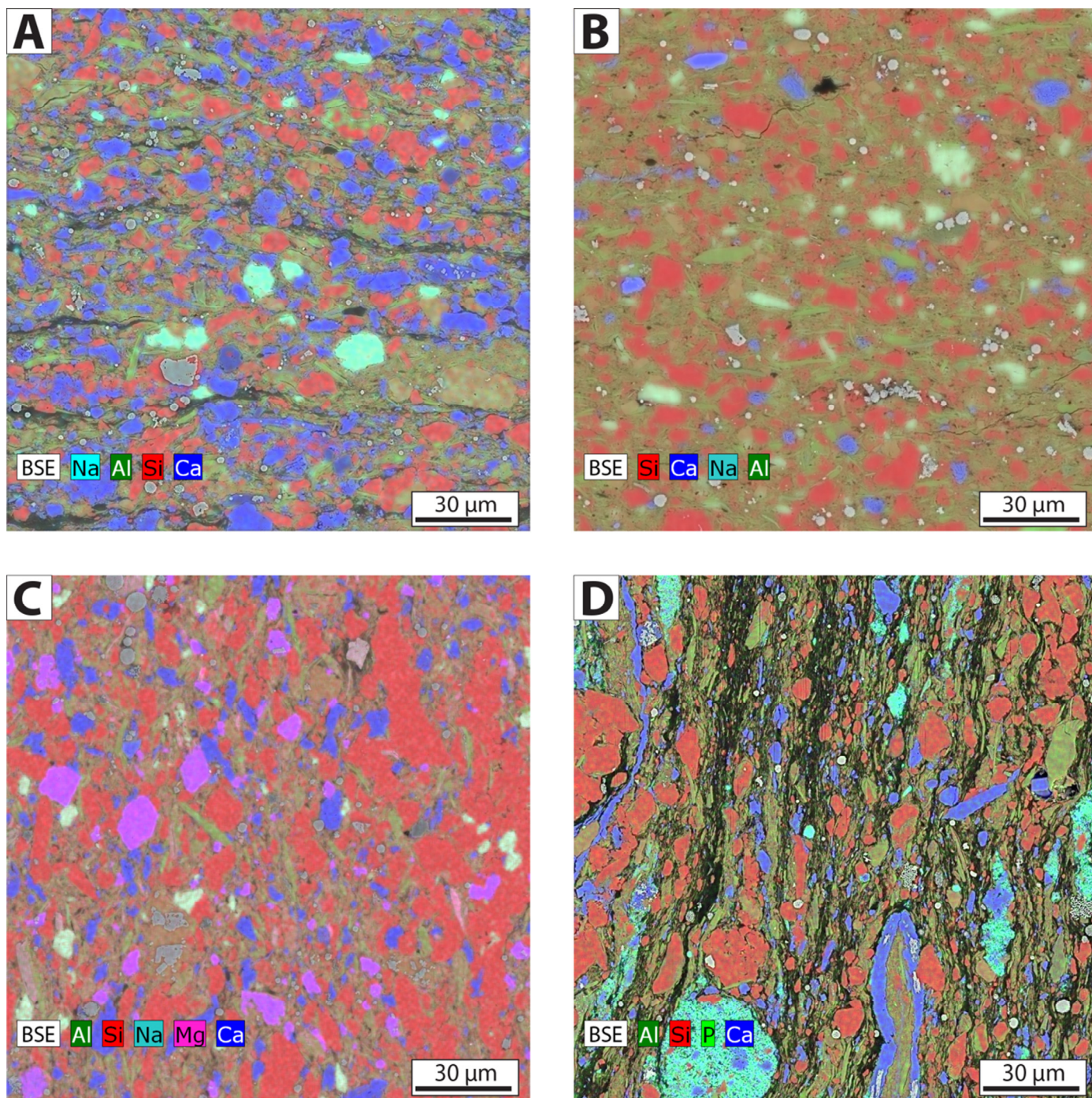


Figure 5. Energy dispersive x-ray spectroscopy (EDS) element maps superimposed on backscattered electron images showing variability in the compositions of mudrock samples from the study. Silica is red; calcite is blue; feldspars, micas, and clay minerals are green; dolomite is purple; albite is aqua; and phosphate is light greenish-blue. (A) Calcite-rich sample with abundant albite. Locker B-2-1 well, 628.25 ft, VRc = 0.53%, TOC = 3.75%. (B) Siliceous-argillaceous sample. Petty D-6-1 well, 1768.8 ft, VRc < 0.7%. (C) Silica-rich sample containing dolomite. Beck C-4-1 well, 1270 ft, VRc = 0.58%, TOC = 3.08%. (D) Organic-matter-rich sample showing higher-than-typical phosphate content. Johanson MC-1 well, 1086 ft, VRc = 0.51%, TOC = 12.72%.

permeability to explain the amount of elemental mobility that would be necessary to account for the magnitude of dissolved and reprecipitated material. The possibility does exist for pores at sizes below the working resolution of our SEM (~5 nm) to have been the network for the aggressive fluids.

CONCLUSIONS

1) The low-thermal-maturity Barnett Shale mudrocks in this study have relatively few pores. The primary reason for this ap-

pears to be the extreme ductility of the kerogen that has filled most interparticle pore spaces.

2) The majority of the pore volume is represented by intraparticle pores, primarily dissolved and/or replaced silt-sized grains, mostly feldspars. Many small interparticle pores are present, particularly between clay mineral grains or where organic matter is absent, but these are rarely volumetrically important. Organic-matter pores are very rare to absent at VR less than 0.75% in the Barnett Shale.

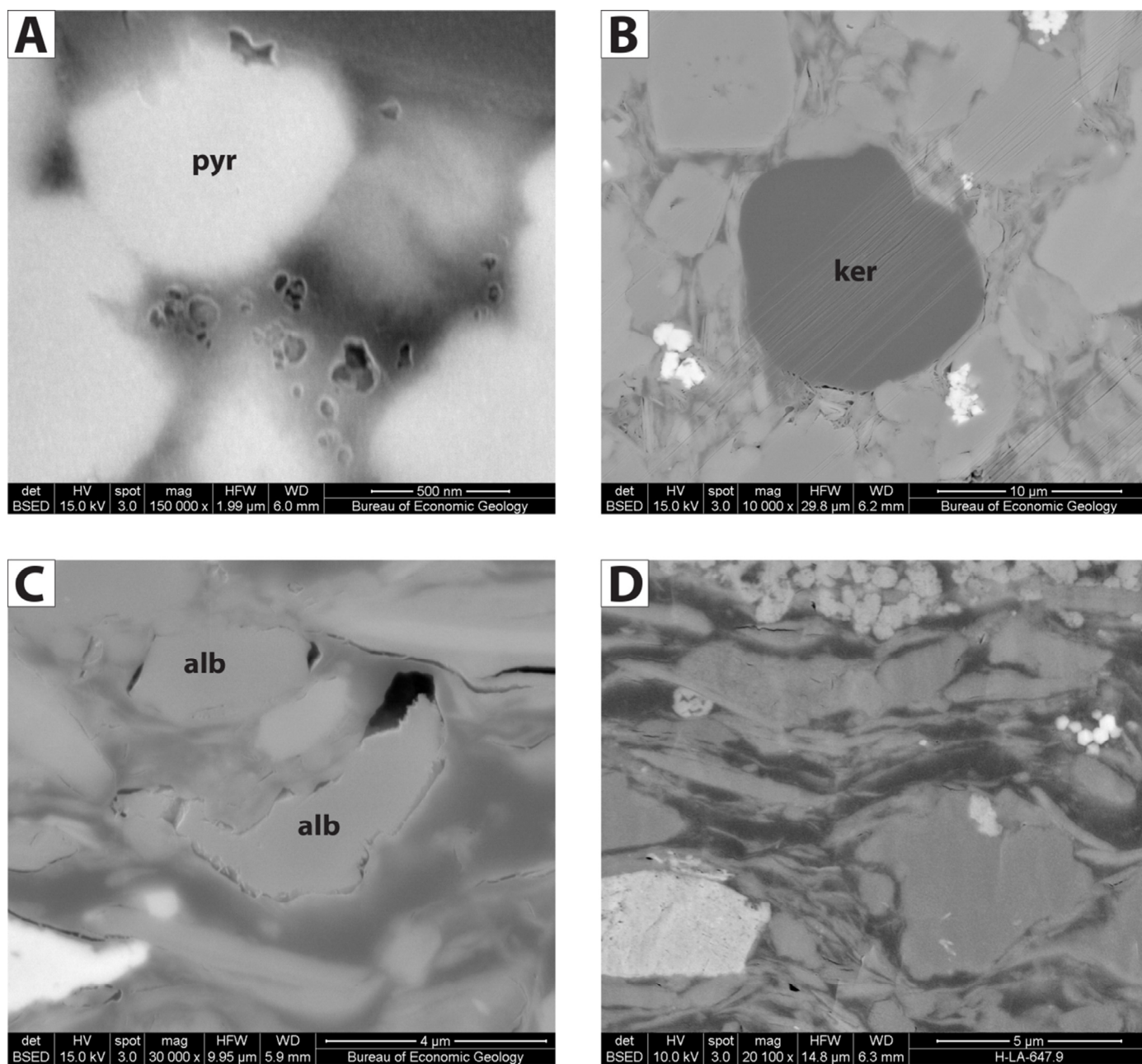


Figure 6. Backscattered electron images showing organic-matter behavior. (A) Image showing rare organic-matter pores within organic matter (bitumen) between the crystals of a pyrite (pyr) framboid. Walker D-1-1 well, 1282 ft, VRc = 0.52%. (B) Image showing an organic-matter grain (rigid kerogen) within a mesh of more ductile organic matter and a few interparticle pores in the stress shadow adjacent to the grain. Diagonal lines are artifacts of the milling process. Beck C-4-1 well, 1270 ft, VRc = 0.58%, TOC = 3.08%. (C) Image showing organic matter surrounding, but not invading, an intraparticle pore related to authigenic albite (alb). Scoggins A-2-1 well, 767 ft, VRc = 0.47%, TOC = 7.57%. (D) Image showing mesh of ductile organic matter (probably kerogen) surrounding grains in a mudrock. Hardy LA-1 well, 647.9 ft, VRc ~ 0.7%.

3) Samples contain mostly ductile kerogen but also some bitumen at higher thermal maturity (near 0.7% VR).

ACKNOWLEDGMENTS

This research was primarily funded by the industrial associates of the Mudrock Systems Research Laboratory at the University of Texas at Austin Bureau of Economic Geology, with additional funding from the State of Texas Advanced Resource Recovery (STARR) project. This paper benefited from reviews by Dr. Ruairi Day-Stirrat and Dr. Mark Rudnicki, and editing by Barry J. Katz and Ling Gao. Steve Ruppel provided assistance with well locations and Rock-Eval data. Technical editing pro-

vided by Stephanie Jones. Publication authorized by the Director, Bureau of Economic Geology.

REFERENCES CITED

- Anders, M. H., S. E. Laubach, and C. H. Scholz, 2014, Microfractures: A review: *Journal of Structural Geology*, v. 69, p. 377–394, doi:10.1016/j.jsg.2014.05.011.
- Ambrose, R. J., R. C. Hartman, M. Diaz-Campos, I. Y. Akkutlu, and C. H. Sondergeld, 2010, New pore-scale considerations for shale gas in place calculations: Society of Petroleum Engineers Paper 131772, Richardson, Texas, 17 p., doi:10.2118/131772-ms.

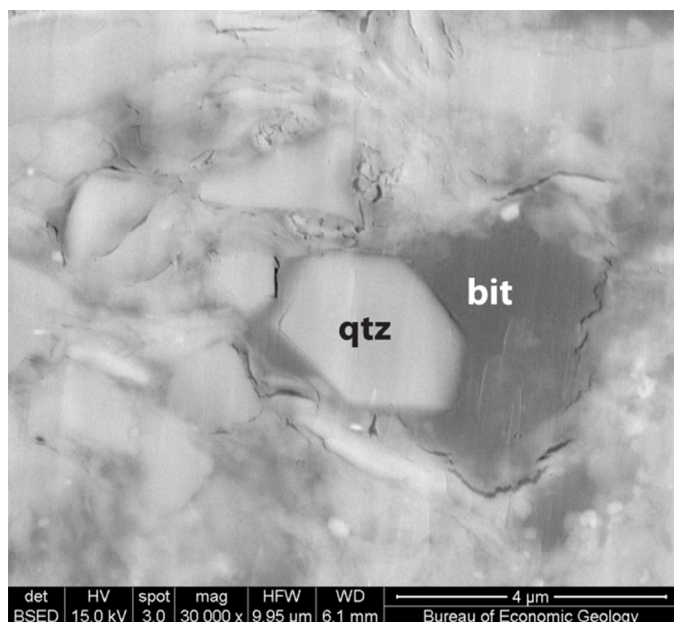


Figure 7. Backscattered electron image showing euheedral quartz cement (qtz) and migrated bitumen (bit). Potter C-9-1 well, 2404.9 ft, VRc < 0.7%.

Bernard, B., R. Wirth, A. Schreiber, H. Schultz, and B. Horsfield, 2012, Formation of nanoporous pyrobitumen residues during maturation of the Barnett Shale (Fort Worth Basin): *International Journal of Coal Geology*, v. 103, p. 3–11, doi:10.1016/j.coal.2012.04.010.

Capuano, R. M., 1993, Evidence of fluid flow in microfractures in geopressed shales: *American Association of Petroleum Geologists Bulletin*, v. 77, p. 1303–1314, doi:10.1306/bdff8e70-1718-11d7-8645000102c1865d.

Cardott, B. J., C. R. Landis, and M. E. Curtis, 2015, Post-oil solid bitumen network in the Woodford Shale, USA—A potential primary migration pathway: *International Journal of Coal Geology*, v. 139, p. 106–113, doi:10.1016/j.coal.2014.08.012.

Chalmers, G. R., R. M. Bustin, and L. M. Power, 2012, Characterization of gas shale pore systems by porosimetry, pycnometry, surface area, and field emission scanning electron microscopy/transmission electron microscopy image analyses: Examples from the Barnett, Woodford, Haynesville, Marcellus, and Doig units: *American Association of Petroleum Geologists Bulletin*, v. 96, p. 1099–1119, doi:10.1306/10171111052.

Curtis, M. E., R. J. Ambrose, C. H. Sondergeld, and C. S. Rai, 2010, Structural characterization of gas shales on the micro- and nanoscales: *Society of Petroleum Engineers Paper 137693*, Richardson, Texas, 15 p., doi:10.2118/137693-MS.

Day-Stirrat, R. J., P. B. Flemings, Y. You, A. C. Aplin, and B. A. van der Pluijm, 2012, The fabric of consolidation in Gulf of Mexico mudstones: *Marine Geology*, v. 295–298, p. 77–85, doi:10.1016/j.margeo.2011.12.003.

Day-Stirrat, R. J., P. B. Flemings, Y. You, and B. A. van der Pluijm, 2013, Modification of mudstone fabric and pore structure as a result of slope failure: Ursa Basin, Gulf of Mexico: *Marine Geology*, v. 341, p. 58–67, doi:10.1016/j.margeo.2013.05.003.

Emmanuel, S., and R. J. Day-Stirrat, 2012, A framework for quantifying size dependent deformation of nano-scale pores in mudrocks: *Journal of Applied Geophysics*, v. 86, p. 29–35, doi:10.1016/j.coal.2012.07.012.

Fishman, N. S., P. C. Hackley, H. A. Lowers, R. J. Hill, S. O. Egenhoff, D. D. Eberl, and A. E. Blum, 2012, The nature of porosity in organic-rich mudstones of the Upper Jurassic Kimmeridge Clay Formation, North Sea, offshore United Kingdom: *International Journal of Coal Geology*, v. 103, p. 32–50, doi:10.1016/j.coal.2012.07.012.

Gale, J. F. W., S. E. Laubach, J. E. Olson, P. Eichhubl, and A. Fall, 2014, Natural fractures in shale: A review and new observa-

tions: *American Association of Petroleum Geologists Bulletin*, v. 98, p. 2165–2216, doi:10.1306/08121413151.

Jarvie, D. M., B. L. Claxton, F. Henk, and J. T. Breyer, 2001, Oil and shale gas from the Barnett Shale, Fort Worth Basin, Texas: *American Association of Petroleum Geologists Annual Meeting Program*, v. 10, p. A100, doi:10.1306/8626e28d-173b-11d7-8645000102c1865d.

Klaver, J., G. Desbois, R. Litke, and J. L. Urai, 2015, BIB-SEM characterization of pore space morphology and distribution in postmature to overmature samples from the Haynesville and Bossier Shales: *Marine and Petroleum Geology*, v. 59, p. 451–466, doi:10.1016/j.marpetgeo.2014.09.020.

Klaver, J., G. Desbois, J. L. Urai, and R. Littke, 2012, BIB-SEM study of the pore space morphology in early mature Posidonia Shale from the Hils area, Germany: *International Journal of Coal Geology*, v. 103, p. 12–25, doi:10.1016/j.coal.2012.06.012.

Lash, G. G., and T. Engelder, 2005, An analysis of horizontal microcracking during catagenesis: Example from the Catskill Delta complex: *American Association of Petroleum Geologists Bulletin*, v. 89, p. 1433–1449, doi:10.1306/05250504141.

Loucks, R. G., and R. M. Reed, 2014, Scanning-electron-microscope petrographic evidence for distinguishing organic matter pores associated with depositional organic matter versus migrated organic matter in mudrocks: *Gulf Coast Association of Geological Societies Journal*, v. 3, p. 51–60.

Loucks, R. G., R. M. Reed, S. C. Ruppel, and U. Hammes, 2012, Spectrum of pore types and networks in mudrocks and a descriptive classification for matrix-related mudrock pores: *American Association of Petroleum Geologists Bulletin*, v. 96, p. 1071–1098, doi:10.1306/08171111061.

Loucks, R. G., R. M. Reed, S. C. Ruppel, and D. M. Jarvie, 2009, Morphology, genesis, and distribution of nanometer-scale pores in siliceous mudstones of the Mississippian Barnett Shale: *Journal of Sedimentary Research*, v. 79, p. 848–861, doi:10.2110/jsr.2009.092.

Loucks, R. G., and S. C. Ruppel, 2007, Mississippian Barnett Shale: Lithofacies and depositional setting of a deep-water shale-gas succession in the Fort Worth Basin, Texas: *American Association of Petroleum Geologists Bulletin*, v. 91, p. 579–601, doi:10.1306/11020606059.

Milliken, K. L., 1992, Chemical behavior of detrital feldspars in mudrocks versus sandstones, Frio Formation (Oligocene), South Texas: *Journal of Sedimentary Research*, v. 62, p. 790–801, doi:10.1306/D42679DD-2B26-11D7-8648000102C1865D.

Milliken, K. L., W. L. Esch, R. M. Reed, and T. Zhang, 2012, Grain assemblages and strong diagenetic overprinting in siliceous mudrocks, Barnett Shale (Mississippian), Fort Worth Basin, Texas: *American Association of Petroleum Geologists Bulletin*, v. 96, p. 1553–1578, doi:10.1306/12011111129.

Milliken, K. L., L. T. Ko, M. Pommer, and K. M. Marsaglia, 2014, SEM petrography of eastern Mediterranean sapropels: Analogue data for assessing organic matter in oil and gas shales: *Journal of Sedimentary Research*, v. 84, p. 961–974, doi:10.2110/jsr.2014.75.

Milliken, K. L., and L. S. Land, 1994, Evidence for fluid flow in microfractures in geopressed shales: Discussion: *American Association of Petroleum Geologists Bulletin*, v. 78, p. 1637–1640, doi:10.1306/a25ff23d-171b-11d7-8645000102c1865d.

Milliken, K. L., and R. M. Reed, 2010, Multiple causes of diagenetic fabric anisotropy in weakly consolidated mud, Nankai accretionary prism, IODP Expedition 316: *Journal of Structural Geology*, v. 32, p. 1887–1898, doi:10.1016/j.jsg.2010.03.008.

Milliken, K. L., M. Rudnicki, D. N. Awwiller, and T. Zhang, 2013, Organic matter-hosted pore system, Marcellus Formation (Devonian), Pennsylvania: *American Association of Petroleum Geologists Bulletin*, v. 97, p. 177–200, doi:10.1306/07231212048.

Peters, K. E., 1986, Guidelines for evaluating petroleum source rock using programmed pyrolysis: *American Association of Petroleum Geologists Bulletin*, v. 70, p. 318–329, doi:10.1306/94885688-1704-11d7-8645000102c1865d.

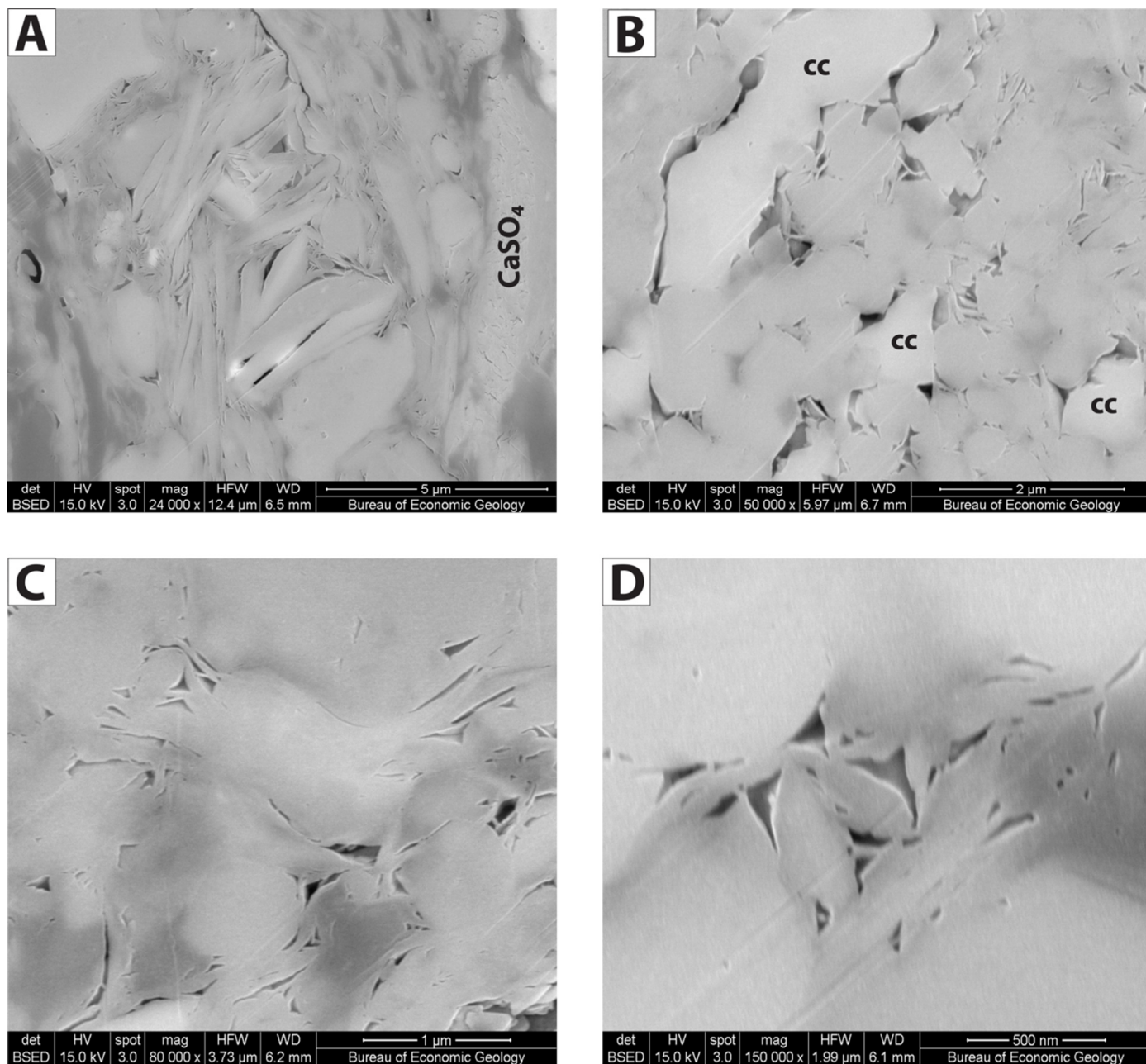
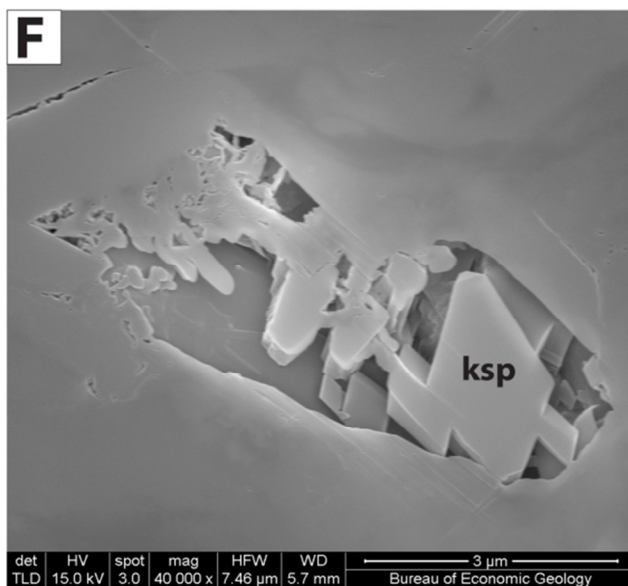
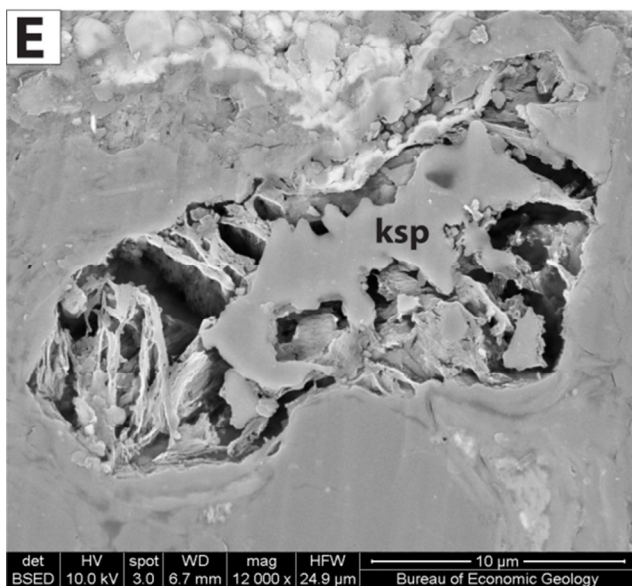
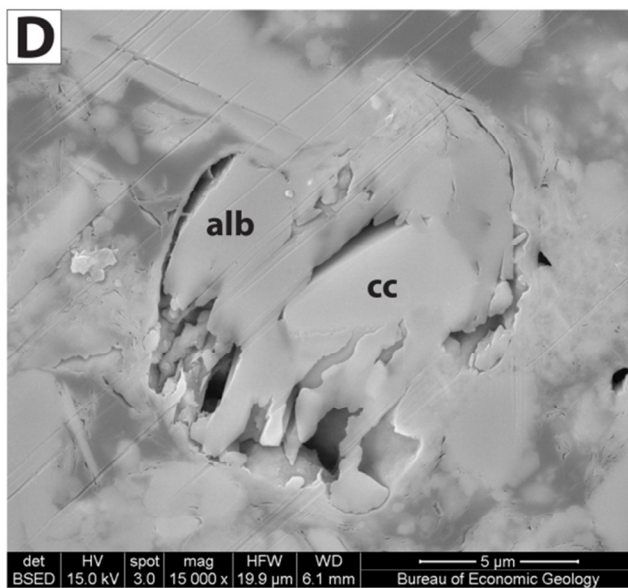
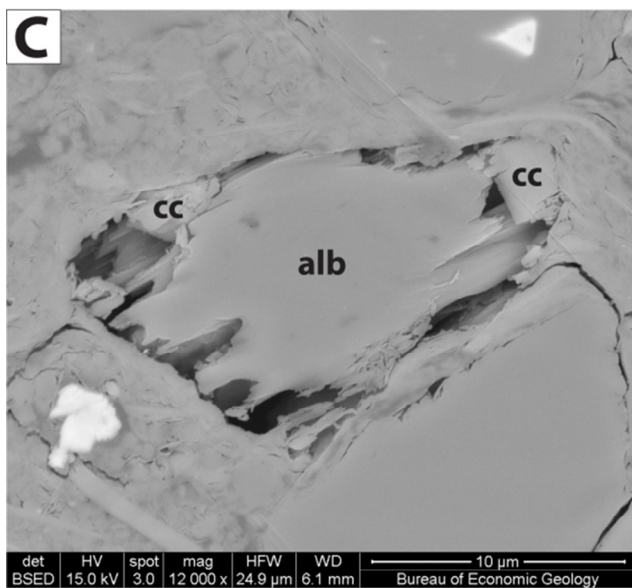
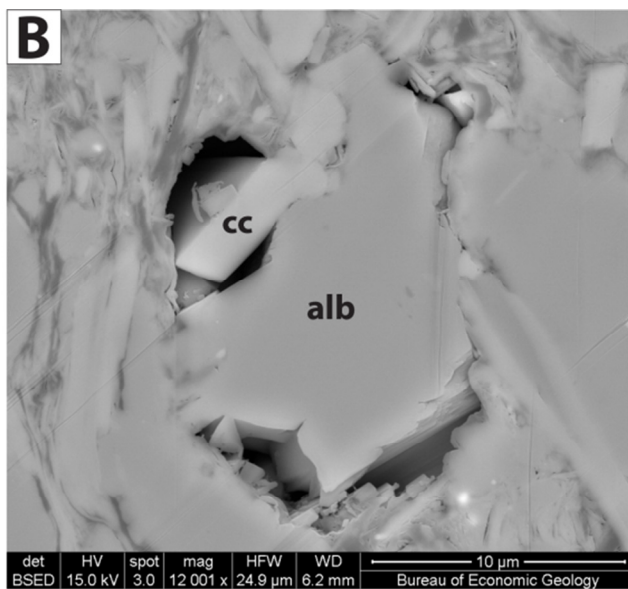
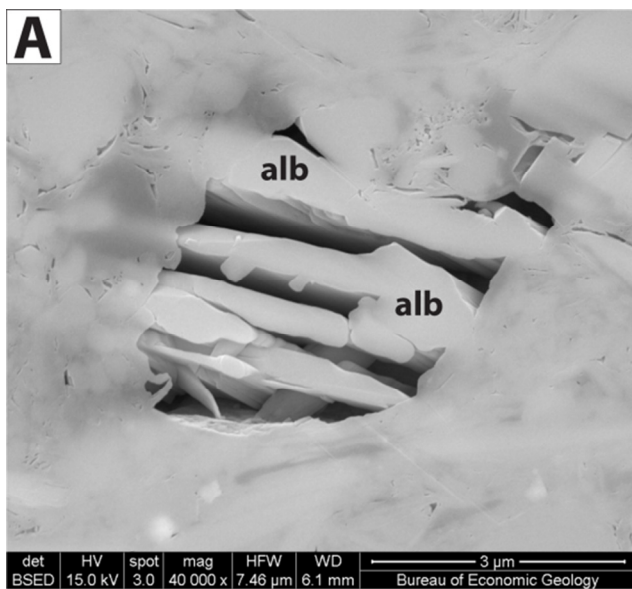


Figure 8. Backscattered electron images showing examples of interparticle pores. (A) Mix of interparticle (triangular) and intraparticle pores in a clay-rich zone. Area on left edge of image is probably a post-coring gypsum-filled microfracture (CaSO_4). Johanson MC-1 well, 1086 ft, VRc = 0.51%, TOC = 12.72%. (B) Image showing interparticle pores in a very-fine-grained and organic-poor area of a mudrock (cc = calcite). Johanson MC-1 well, 1070 ft, VRc = 0.62%, TOC = 3.17%. (C) Image showing primarily interparticle pores, some of which are in stress shadows around grains. Johanson MC-1 well, 1070 ft, VRc = 0.62%, TOC = 3.17%. (D) High-magnification image showing primarily interparticle pores between clay mineral grains. Locker B-2-1 well, 603.1 ft, VRc = 0.47%, TOC = 7.57%.

(Facing Page) Figure 9. SEM images of intraparticle pores related to dissolution and/or replacement of detrital feldspar grains. (A) Backscattered electron image showing albite (alb) partially replacing a dissolved feldspar grain. Petty D-6-1 well, 1768.8 ft, VR < 0.7%. (B) Backscattered electron image showing albite (alb) and calcite (cc) partially replacing a feldspar grain. Beck C-4-1 well, 1270 ft, VRc = 0.58%, TOC = 3.08%. (C) Backscattered electron image showing albite (alb) and calcite (cc) replacing a feldspar grain. Johanson MC-1 well, 1070 ft, VRc = 0.62%, TOC = 3.17%. (D) Backscattered electron image showing albite (alb) and calcite (cc) replacing a feldspar grain. Locker B-2-1 well, 603.1 ft, VRc = 0.47%, TOC = 7.57%. (E) Backscattered electron image showing partially-dissolved K-feldspar (ksp) and authigenic clay. Godfrey E-8-1 well, 2400.5 ft, VRc < 0.7%. (F) Secondary electron image showing partially-euhedral K-feldspar (ksp) and minor clay minerals related to intraparticle pores. Beck C-4-1 well, 1254.33 ft, VRc = 0.58%, TOC = 3.75%.



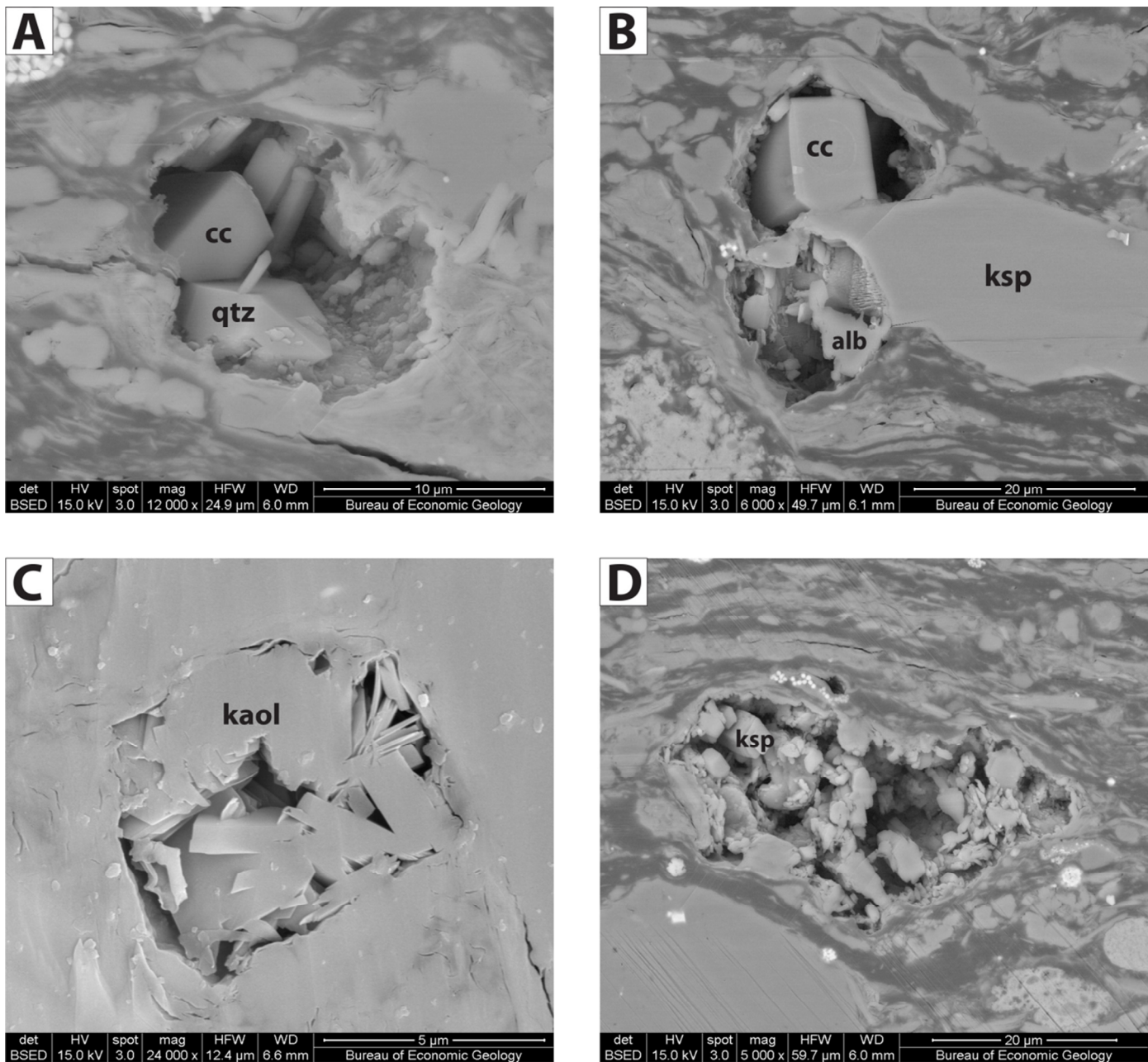


Figure 10. Backscattered electron images showing intraparticle pores related to dissolution, replacement, and reprecipitation of chemically unstable grains, some of which may have been rock fragments. (A) Image showing dissolved grain mold being partially cemented with euhedral calcite (cc) and quartz (qtz). Johanson MC-1 well, 1086 ft, VRc = 0.51%, TOC = 12.72%. (B) Image showing complicated pore system including calcite (cc) partially filling an intraparticle pore from a dissolved grain, a partially-dissolved K-feldspar (ksp), and albite (alb) partially replacing a feldspar grain. Johanson MC-1 well, 1086 ft, VRc = 0.51%, TOC = 12.72%. (C) Image showing kaolinite (kaol) partially replacing grain. Moore C-1-1 well, 189.9 ft, VRc \approx 0.5%. (D) Image showing K-feldspar (ksp) and clay minerals as remnants of a dissolved grain. Johanson MC-1 well, 1086 ft, VRc = 0.51%, TOC = 12.72%.

Pollastro, R. M., D. M. Jarvie, R. J. Hill, and C. W. Adams, 2007, Geologic framework of the Mississippian Barnett Shale, Barnett-Paleozoic total petroleum system, Bend Arch-Fort Worth Basin, Texas: American Association of Petroleum Geologists Bulletin, v. 91, p. 405-436, doi:10.1306/10300606008.

Romero-Sarmiento, M.-F., M. Ducros, B. Carpentier, F. Lorant, M.-C. Cacas, S. Pegaz-Fiornet, S. Wolf, S. Rohais, I. Moretti, 2013, Quantitative evaluation of TOC, organic porosity and gas retention distribution in a gas shale play using petroleum system modeling: Application to the Mississippian Barnett Shale: Marine and Petroleum Geology, v. 45, p. 315-330, doi:10.1016/j.marpetgeo.2013.04.003.

Schieber, J., 2010, Common themes in the formation and preservation of intrinsic porosity in shales and mudstones—Illustrated with examples across the Phanerozoic: Society of Petroleum Engineers Unconventional Gas Conference, Pittsburgh, Pennsylvania, USA: Society of Petroleum Engineers Paper 132370, Richardson, Texas, 10 p., doi:10.2118/132370-m.

Schieber, J., R. Lazar, K. Bohacs, B. Klimentidis, J. Ottmann, and M. Dumitrescu, in press, An SEM study of porosity in the Eagle Ford Shale of Texas—Pore types and porosity distribution in a depositional and sequence stratigraphic context: American Association of Petroleum Geologists Memoir, Tulsa, Oklahoma.

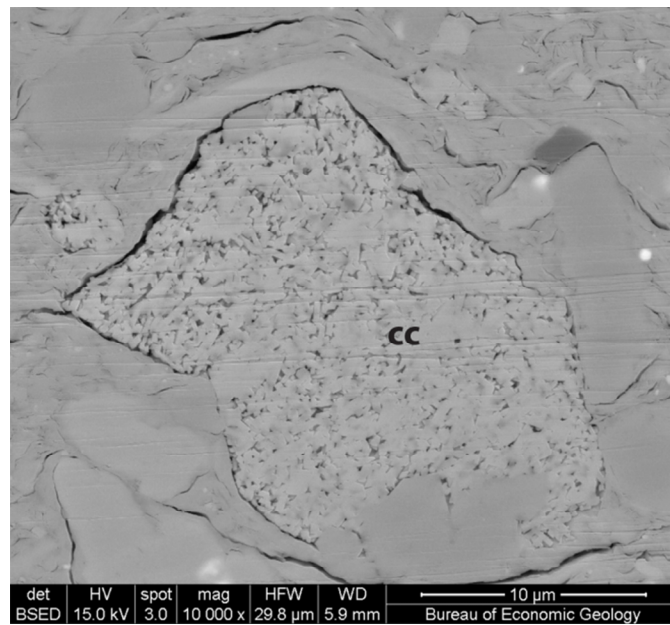


Figure 11. Backscattered electron image showing calcite (cc) grain (either a pellet or a clast from the shelf) containing intraparticle pores. Neal A-1-1 well, 362 ft, VRc = 0.63%, TOC = 0.95%.

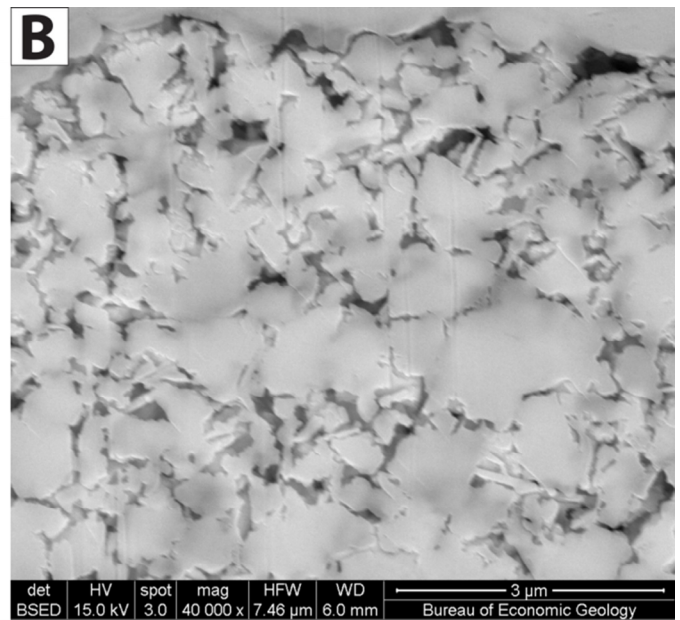
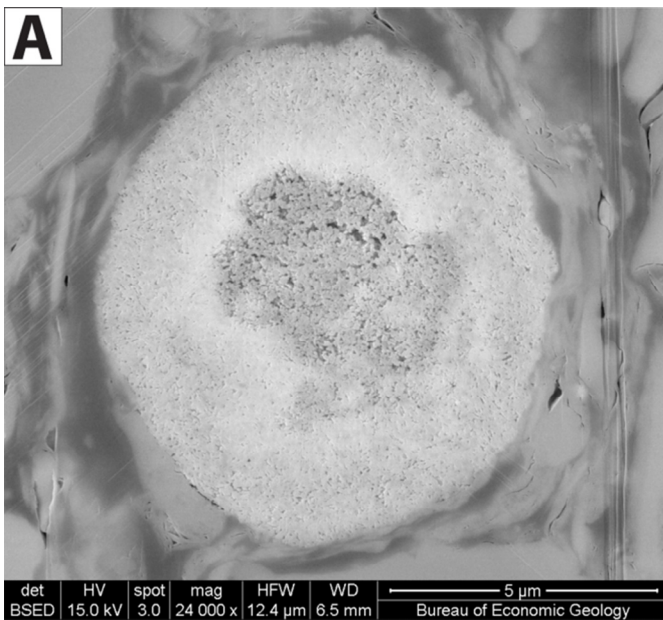


Figure 12. Backscattered electron images showing pores related to phosphate. (A) Image showing intraparticle pores in a phosphate grain. Johanson MC-1 well, 1086 ft, VRc = 0.51%, TOC = 12.72%. (B) Image showing intraparticle pores that resemble interparticle pores, in a partially-compacted phosphate-clay pellet. Neal A-1-1 well, 396 ft, VRc = 0.67%, TOC = 2.36%.

Schneider, J., P. B. Flemings, R. J. Day-Stirrat, and J. T. Germaine, 2011, Insights into porescale controls on mudstone permeability

through resedimentation experiments: *Geology*, v. 39, p. 1011–1014, doi:10.1130/g32475.1.

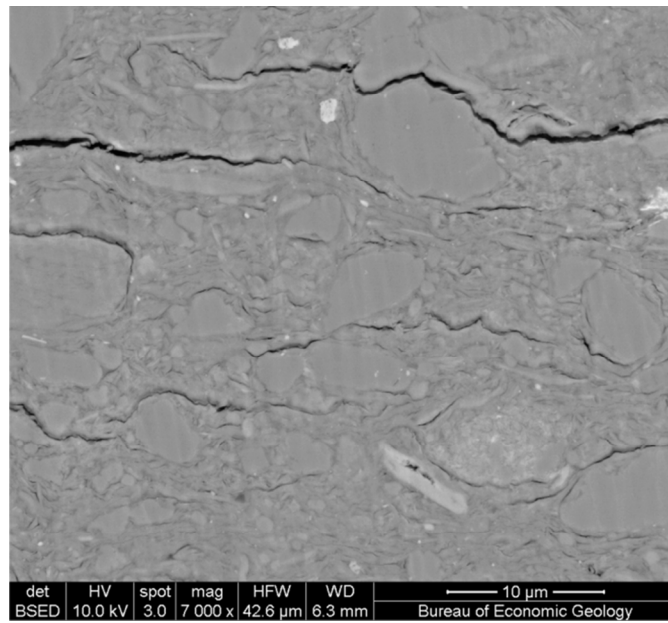


Figure 13. Backscattered electron image showing open stress-release microfractures in a clay-mineral-rich mudrock. Neal A-1-1 well, 385.6 ft, VR \approx 0.6%.

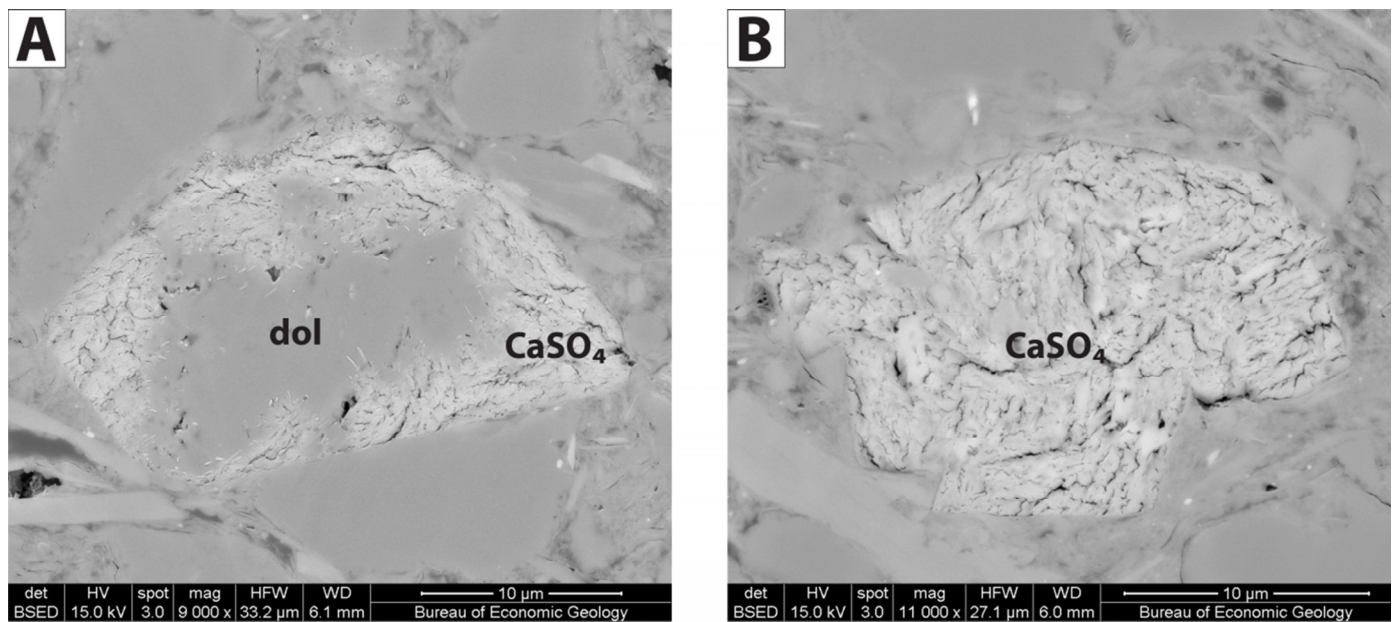


Figure 14. Backscattered electron images showing alteration of grains to porous Ca-sulfate. (A) Image showing partially-altered dolomite (dol) core surrounded by Ca-sulfate (CaSO₄). (B) Image showing grain, probably originally dolomite based on crystal faces along bottom of particle, completely altered to Ca-sulfate (CaSO₄). Both images from Petty D-6-1 well, 1768.8 ft, VR < 0.7%.